


# Nomogram Development and Validation for Predicting Postoperative Recurrent Lumbar Disc Herniation Based on Paraspinal Muscle Parameters

Ming Tang<sup>1,2,\*</sup>, Siyuan Wang<sup>1,2,\*</sup>, Yiwen Wang<sup>1</sup>, Fanyi Zeng<sup>1</sup>, Mianpeng Chen<sup>1</sup>, Xindong Chang<sup>1</sup>, Mingfei He<sup>1</sup>, Qingqing Fang<sup>1</sup>, Shiwu Yin<sup>1</sup> 

<sup>1</sup>Department of Interventional Vascular Medicine, Hefei Hospital Affiliated to Anhui Medical University, The Second People's Hospital of Hefei, Hefei City, Anhui Province, People's Republic of China; <sup>2</sup>The Fifth Clinical College of Medicine, Anhui Medical University, Hefei City, Anhui Province, People's Republic of China

\*These authors contributed equally to this work

Correspondence: Shiwu Yin, Department of Interventional Vascular Medicine, Hefei Hospital Affiliated to Anhui Medical University, The Second People's Hospital of Hefei, 574 Changjiang East Road, Yaohai District, Hefei City, Anhui Province, 230011, People's Republic of China, Email yinshiwu@126.com

**Purpose:** Previous studies highlight paraspinal muscles' significance in spinal stability. This study aims to assess paraspinal muscle predictiveness for postoperative recurrent lumbar disc herniation (PRLDH) after lumbar disc herniation patients undergo percutaneous endoscopic transforaminal discectomy (PETD).

**Patients and Methods:** Retrospectively collected data from 232 patients undergoing PETD treatment at our institution between January 2020 and January 2023, randomly allocated into training (60%) and validation (40%) groups. Utilizing Lasso regression and multivariable logistic regression, independent risk factors were identified in the training set to construct a Nomogram model. Internal validation employed Enhanced Bootstrap, with Area Under the ROC Curve (AUC) assessing accuracy. Calibration was evaluated through calibration curves and the Hosmer-Lemeshow goodness-of-fit test. Decision curve analysis (DCA) and clinical impact curve (CIC) were employed for clinical utility analysis.

**Results:** Diabetes, Modic changes, and ipsilesional multifidus muscle skeletal muscle index (SMI) were independent predictive factors for PRLDH following PETD ( $P < 0.05$ ). Developed Nomogram model based on selected predictors, uploaded to a web page. AUC for training: 0.921 (95% CI 0.872–0.970), validation: 0.900 (95% CI 0.828–0.972), respectively. The Hosmer-Lemeshow test yielded  $\chi^2 = 5.638/6.259$ ,  $P = 0.688/0.618$ , and calibration curves exhibited good fit between observed and predicted values. DCA and CIC demonstrate clinical net benefit for both models at risk thresholds of 0.02–1.00 and 0.02–0.80.

**Conclusion:** The Nomogram predictive model developed based on paraspinal muscle parameters in this study demonstrates excellent predictive capability and aids in personalized risk assessment for PRLDH following PETD.

**Keywords:** lumbar disc herniation, percutaneous endoscopic transforaminal discectomy, postoperative recurrent lumbar disc herniation, predictive model

## Introduction

Intervertebral disc-related low back pain (LBP), comprising 39% of all cases, is mainly attributed to disc herniation (approximately 30%), with other causes being less common.<sup>1</sup> Lumbar disc herniation (LDH) occurs when the fibrous ring of an intervertebral disc ruptures, leading to the protrusion and exposure of the nucleus pulposus in the surrounding fluid.<sup>2</sup> This leads to inflammation and compression of nerve roots, causing nerve root damage and subsequent symptoms such as lower back and leg pain.<sup>3</sup> In recent years, percutaneous endoscopic transforaminal discectomy (PETD) has emerged as a preferred minimally invasive treatment for LDH. PETD offers advantages such as minimal trauma, fewer

complications, and quicker recovery.<sup>4</sup> However, postoperative recurrent lumbar disc herniation (PRLDH) remains a concern, with an incidence ranging from 3–16% according to the literature.<sup>5–7</sup>

The spine's stability depends on the passive subsystem (vertebrae, intervertebral discs, facet joints, spinal ligaments), active subsystem (paraspinal muscles), and neural control subsystem, which are both independent and interconnected.<sup>8</sup> Therefore, impairment in any of these components can result in reduced spinal function. Crisco et al<sup>9</sup> conducted load-bearing experiments on cadaveric lumbar vertebrae with muscles removed, retaining only the ligaments. They observed that lumbar stability decreased when subjected to an average load of 88N, whereas the intact lumbar system in a living body could withstand an average load of 2600N. To explore the impact of paraspinal muscles on PRLDH, we reviewed the relevant literature and found that magnetic resonance imaging (MRI) is one of the gold standard methods for assessing whole-body and local skeletal muscle mass, subcutaneous fat tissue and visceral fat tissue, and for LDH patients, MRI can not only assess intervertebral disc degeneration (IVDD), but also observe the relationship between protruding intervertebral disc and nerve root.<sup>10,11</sup> This presents an opportunity to evaluate skeletal muscle mass using MRI. Several studies have demonstrated a correlation between MRI-measured paraspinal muscle fat infiltration, IVDD, and LBP.<sup>12,13</sup> Such infiltration leads to a loss of functional muscle, affecting spinal stability. Therefore, this study aims to investigate the impact of paraspinal functional muscle, assessed via MRI, and other factors on the occurrence of PRLDH after PETD, and to develop and validate the corresponding Nomogram, so that the risk of PRLDH can be more accurately assessed in clinical work. This study strictly adheres to the guidelines of the “Transparent Reporting of a Multivariable Prediction Model for Individual Prognosis or Diagnosis (TRIPOD)”, with [Supplementary Figure S2](#) providing detailed information.

## Materials and Methods

### Patients

This retrospective study included 232 patients diagnosed with LDH who were admitted to our hospital between January 2020 and January 2023. The inclusion criteria were as follows: (1) patients met the diagnostic criteria for LDH;<sup>4</sup> (2) a minimum symptom duration of at least 3 months, with MRI diagnosis consistent with clinical manifestations and signs, and conservative treatment proving ineffective; (3) PETD treatment planned (see [Supplementary information S1](#) for detailed surgical procedure), with significant postoperative symptom relief. Exclusion criteria were as follows: (1) previous lumbar spine surgeries; (2) concurrent spinal conditions such as tumors, tuberculosis, deformities, and fractures affecting spinal structure; (3) long-term use of medications affecting paraspinal muscles after surgery; (4) uncertainty regarding the affected disc; (5) incomplete clinical data; (6) significant cardiovascular or cerebrovascular diseases, or other congenital disorders. PRLDH is characterized by significant alleviation of postoperative neurological symptoms, succeeded by a recurrence of nerve compression symptoms at the same segment and side, confirmed via imaging examinations, around six months post-surgery.<sup>14</sup> The follow-up duration spanned 6 months, primarily conducted through outpatient visits, electronic medical record tracking, and telephone interviews.

### Imaging Assessment Method

#### Paraspinal Muscle

All patients underwent preoperative MRI (3.0T, Siemens, Germany) in a supine position to obtain T2-weighted axial images (see [Supplementary information S2](#) for details). As reported in the literature, the maximum cross-sectional area (CSA) of the paraspinal muscles is located between the L3/4 and L4/5 disc levels, while the largest CSA of the psoas major muscle is at the L4/5 disc level.<sup>15,16</sup> Hence, we selected the paraspinal muscles at the level of the L4/5 intervertebral disc. The T2-weighted images were imported into Image J software. Two experienced radiologists (reader 1, with 8 years of MRI diagnostic experience; reader 2, with 4 years of MRI diagnostic experience) independently measured the preoperative contralateral and ipsilateral multifidus CSA, erector spinae CSA, and psoas major CSA. The fat CSA of the contralateral and ipsilateral multifidus, erector spinae, and psoas major were measured. Mean values were used for statistical analysis ([Figure 1](#)). The functional cross-sectional area (FCSA) of the paraspinal muscles was calculated as  $FCSA = \text{Paraspinal Muscle CSA} - \text{Paraspinal Muscle Fat CSA}$ . Additionally, to control for inter-individual size differences, the FCSA was

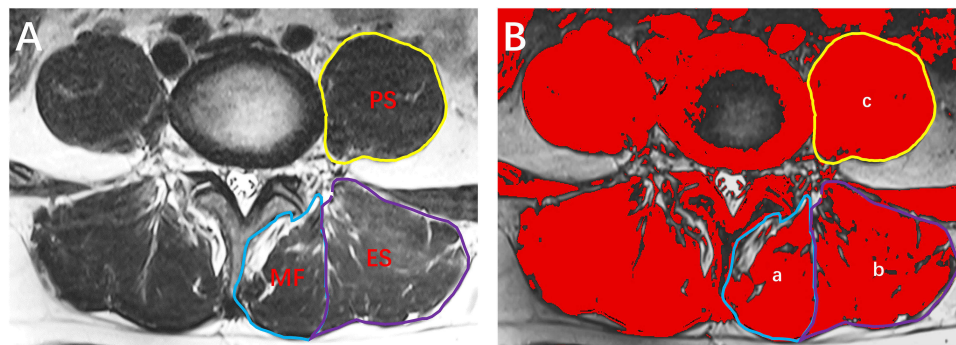


**Figure 1** L4/5 paraspinous muscles at the lumbar interspace. **(A)** T2-weighted images (MF: Multifidus muscle; ES: Erector spinae; PS: Psoas major). **(B)** Computation of paraspinous muscle cross-sectional area and fatty infiltration area (a: Multifidus muscle; b: Erector spinae; c: Psoas major).

transformed into the standardized functional cross-sectional area (SFCSA), given by  $SFCSA = \text{Paraspinal Muscle FCSCA} / \text{Corresponding Vertebral Body CSA} \times 100\%$ . To further normalize for different heights among patients, the paraspinous muscles' skeletal muscle index (SMI) was calculated as  $SMI = \text{Paraspinal Muscle FCSCA (mm}^2) \div \text{Height}^2 \text{ (m}^2)$ .<sup>17</sup>

### Vertebral Bodies and Facet Joints

Using T2-weighted sagittal MRI images, we measured the IA between the upper and lower vertebral bodies of the affected disc, and by subtracting the IAs of the upper and lower vertebral bodies, we obtained the intervertebral disc angle (IDA) (Figure 2). Additionally, using CT axial images (MX8000, MACONI, USA), we measured the facet joint angle (FJA) of the affected disc. The FJA was determined as the angle between the line connecting the anterior and posterior points of the facet joint and the tangent to the posterior margin of the vertebral body at the lower level of the intervertebral disc (Figure 2).

### Risk Factors

The included risk factors were as follows: General characteristics: age, gender, height, body mass index (BMI), diabetes, hypertension, smoking, drinking, preoperative visual analog scale (VAS) score, postoperative VAS score, educational level, occupation, course of disease, hospital stay, and duration of surgery. Imaging features: Pfirrmann grade, Modic changes, IDA, left and right FJA, contralesional multifidus muscle's SFCSA and SMI, ipsilesional multifidus muscle's SFCSA and SMI, contralesional erector spinae muscle's SFCSA and SMI, ipsilesional erector spinae muscle's SFCSA

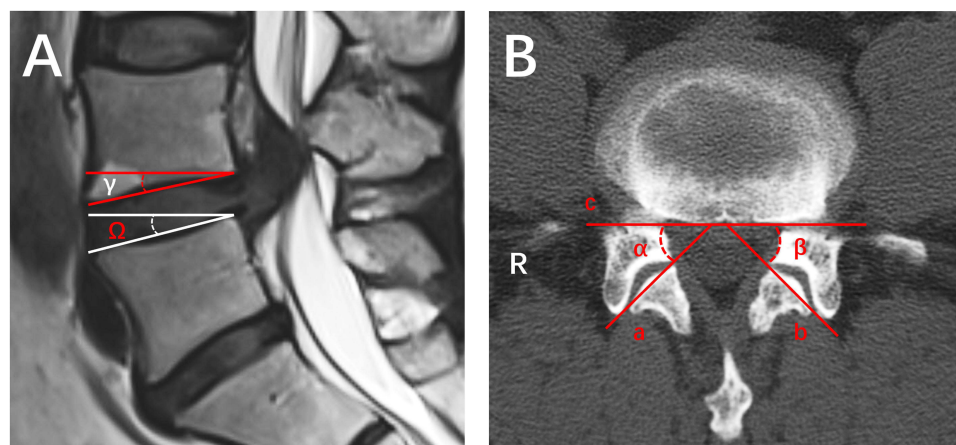


**Figure 2** **(A)** T2-weighted MRI.  $\gamma$ : Upper vertebral endplate inclination angle (IA);  $\Omega$ : Lower vertebral endplate IA; Intervertebral disc angle (IDA) =  $\gamma - \Omega$ . **(B)** c: Tangent to the posterior edge of the vertebral body; ab: Line connecting the facet joints (F) anterior-medial point and the Fj's posterior-lateral point; Right facet joint angle (FJA): Angle  $\alpha$  formed by points a and c; Left FJA: Angle  $\beta$  formed by points b and c.

and SMI, contralesional psoas major muscle's SFCSA and SMI, ipsilesional psoas major muscle's SFCSA and SMI, herniation type, and herniation segments.

## Statistical Analysis

Statistical analyses were conducted using R Studio software (v4.2.3, <http://www.rproject.org/>). The “irr” package was employed to compute the intraclass correlation coefficient (ICC), with results  $\geq 0.75$  indicating good consistency. The “glmnet” package performed Least Absolute Shrinkage and Selection Operator (LASSO) regression for the selection of predictive factors for PRLDH occurrence. Multiple logistic regression was carried out using the “rms” package. The “nomogramFormula” package was utilized to create the Nomogram. Calibration curves and the Hosmer-Lemeshow goodness-of-fit test were generated using the “rms” package. Decision Curve Analysis (DCA) and Clinical Impact Curve (CIC) were plotted using the “rmda” package. Statistical significance was set at  $P < 0.05$ . All modifications to the typeface and font size of the figures were made using Adobe Illustrator. Additional details are available in [Supplementary Information S3](#).<sup>18</sup>

## Results

### Comparison of Clinical Data Between Two Groups

This study included 232 patients, comprising 140 males and 92 females, with an age range of 21 to 83 years (mean age:  $52.94 \pm 13.88$  years). Among these patients, 26 experienced PRLDH, resulting in a recurrence rate of 11.21%. Clinical information for recurrent and non-recurrent patients is compared in [Supplementary Tables S1](#) and [S2](#). Excellent consistency in data measurements between the two observers was observed (0.847–0.922, [Supplementary Table S3](#)). Using the “caret” package in R, random sampling was performed with the createDataPartition function, dividing collected cases into training (n=140) and validation (n=92) sets in a 6:4 ratio ([Table 1](#)).

**Table 1** Characteristics of Training and Validation Groups

Characteristics	Training (n=140)	Validation (n=92)	t/z/ $\chi^2$	P
<b>Age</b>	53.35±13.82	52.33±14.02	0.549	0.584
<b>Gender (Male)</b>	78(55.71%)	62(67.39%)	2.694	0.101
<b>BMI (kg/m<sup>2</sup>)</b>	24.35±2.83	24.44±2.64	0.240	0.811
<b>Height (cm)</b>	165.60±7.41	168.20±8.30	2.530	<b>0.012<sup>#</sup></b>
<b>Diabetes</b>	12(8.57%)	12(13.04%)	0.764	0.382
<b>Hypertension</b>	31(22.14%)	32(34.78%)	3.868	<b>0.049<sup>#</sup></b>
<b>Smoking</b>	47(33.57%)	30(32.61%)	<0.001	0.992
<b>Drinking</b>	30(21.43%)	15(16.30%)	0.633	0.426
<b>Preoperative VAS score*</b>	5(5, 6)	5(5, 6)	7.591	0.128
<b>Postoperative VAS score*</b>	2(2, 3)	2(2,3)	6.476	0.321
<b>Educational level</b>			3.835	0.147
Primary school≤	50(35.71%)	22(23.91%)		
Secondary and High school	66(47.14%)	49(53.26%)		
≥College	24(17.14%)	21(22.82%)		
<b>Occupation</b>			9.349	0.053
Unemployed	39(27.86%)	24(26.09%)		
Laborer	13(9.29%)	19(20.65%)		
Farmer	44(31.43%)	27(29.35%)		
Office worker	25(17.86%)	16(17.39%)		
Self-employed households	19(13.57%)	16(17.39%)		
<b>Course of disease (months)*</b>	19.5(5, 60)	12(3, 75)	6.853	0.904
<b>Hospital stay (days)*</b>	11.34±2.71	11.83±3.33	1.214	0.226
<b>Duration of surgery (min)</b>	69.15±11.17	70.37±12.11	0.787	0.432

(Continued)

Table I (Continued).

Characteristics	Training (n=140)	Validation (n=92)	t/z/ $\chi^2$	P
<b>Pfirrmann grade</b>			3.021	0.554
I	20(14.29%)	11(7.86%)		
II	74(52.86%)	54(58.70%)		
III	45(32.14%)	26(28.26%)		
IV	1(0.71%)	0(0.00%)		
V	0(0.00%)	1(1.09%)		
<b>Modic change</b>			7.618	0.055
Nomral	104(74.29%)	59(64.13%)		
Type I	0(0.00%)	4(4.35%)		
Type II	33(23.57%)	27(29.35%)		
Type III	3(2.14%)	2(2.17%)		
<b>IDA</b>	8.22±5.17	8.91±4.47	1.039	0.300
<b>Left FJA (°)</b>	45.31±10.71	43.31±10.39	1.407	0.161
<b>Right FJA (°)</b>	46.77±12.12	44.87±12.25	1.168	0.244
<b>SFCSA (%)</b>				
Contralesional multifidus	37.67±13.13	37.53±14.93	0.072	0.942
Ipsilesional multifidus	36.43±13.32	37.30±14.43	0.471	0.638
Contralesional erector spinae	47.09±16.96	49.79±19.91	1.104	0.271
Ipsilesional erector spinae	47.02±18.02	49.65±20.01	1.041	0.299
Contralesional psoas major	65.14±17.73	64.67±21.62	0.177	0.860
Ipsilesional psoas major	65.37±17.99	65.95±24.31	0.210	0.834
<b>SMI (mm<sup>2</sup>/m<sup>2</sup>)</b>				
Contralesional multifidus	286.98±101.56	277.10±105.64	0.713	0.477
Ipsilesional multifidus	277.95±102.587	275.41±102.97	0.185	0.854
Contralesional erector spinae	364.59±148.80	372.00±150.02	0.372	0.710
Ipsilesional erector spinae	364.63±155.58	373.80±166.02	0.428	0.669
Contralesional psoas major	504.60±167.40	484.30±178.84	0.880	0.380
Ipsilesional psoas major	507.00±169.91	492.70±183.61	0.609	0.543
<b>Herniation type</b>			<0.001	1.000
Herniation	95(67.86%)	62(67.39%)		
Prolapse	45(32.14%)	30(32.61%)		
<b>Herniation Segments</b>			1.150	0.563
L4/5	75(45.71%)	45(60.87%)		
L5/S1	53(47.86%)	41(29.35%)		
Others	12(6.43%)	6(9.78%)		

**Notes:** \*Median (P25, P75); #Bold font indicates statistical significance.

**Abbreviations:** BMI, Body Mass Index; IDA, Intervertebral Disc Angle; FJA, Facet Joint Angle; SFCSA, Standardized Functional Cross-Sectional Area = Paraspinal Muscle FCSA / Same-Level Vertebral Surface Area × 100%; SMI, Skeletal Muscle Index = Paraspinal Muscle FCSA (mm<sup>2</sup>) / Height<sup>2</sup> (m<sup>2</sup>).

## Model Development

To prevent overfitting, each feature requires participation from at least 10–15 patients in model construction.<sup>19,20</sup> Given the training group's 140 patients, the maximum feature limit is set at 14. Utilized Lasso regression for variable selection. The model exhibited optimal performance ( $\lambda = 0.056$ ) with four predictors (Figure 3). Diabetes, Modic changes, ipsilesional multifidus SMI, and ipsilesional erector spinae SMI were incorporated into a multivariable logistic regression model. Ultimately, diabetes, Modic changes, and ipsilesional multifidus SMI ( $P < 0.05$ ) emerged as independent predictors for PRLDH post-PETD (Table 2). Developed a Nomogram model with these predictors (Figure 3) and made it available at [https://sofarnomogram.shinyapps.io/DynNo\\_PRLDH/](https://sofarnomogram.shinyapps.io/DynNo_PRLDH/).

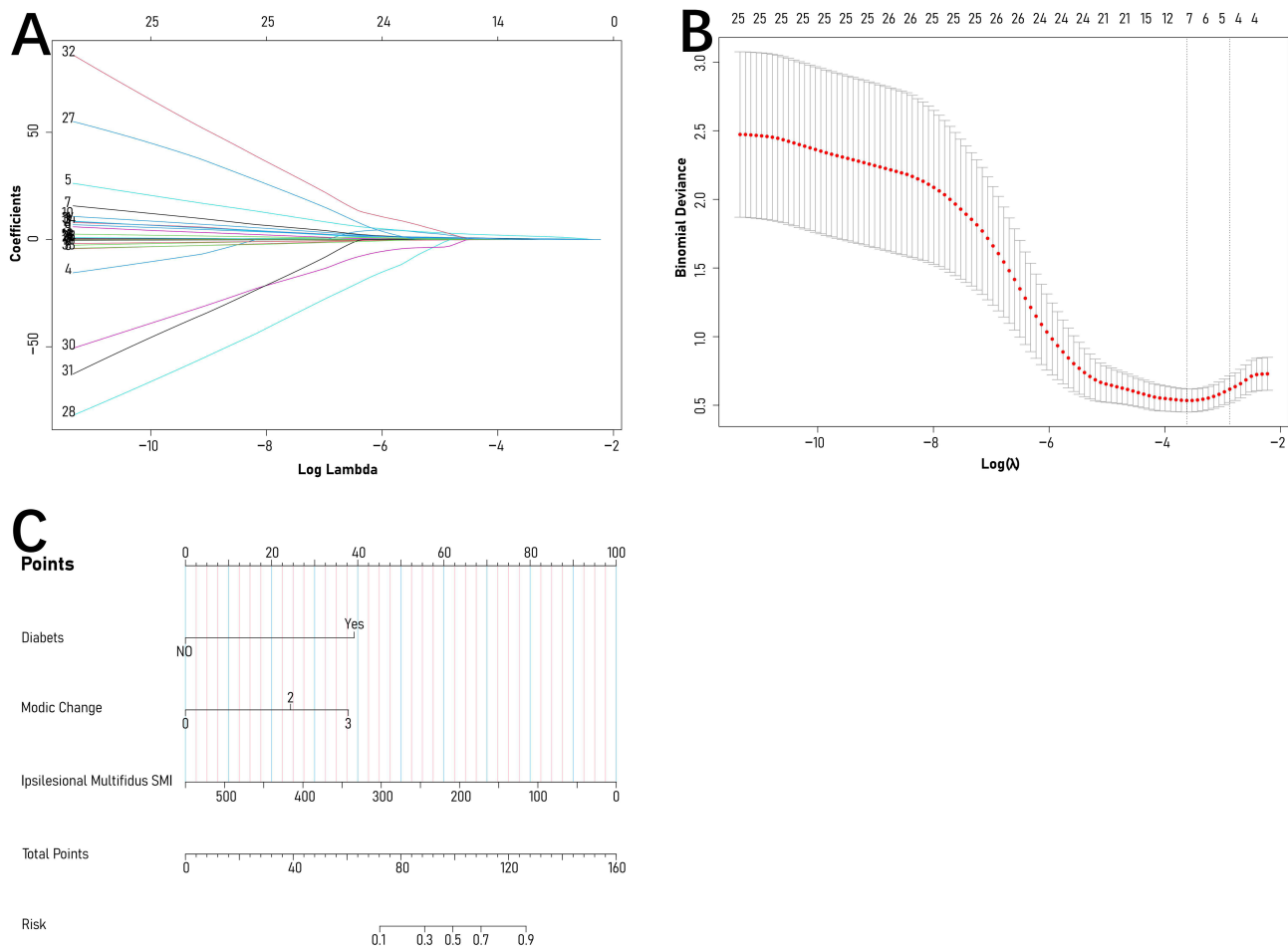


**Figure 3** (A) Characterizing the Variations of LASSO Regression Coefficients. (B) LASSO regression selects the optimal parameter lambda through cross-validation. The dashed line on the right represents lambda values with average error within  $\pm 1$  standard deviation, indicating improved model performance. (C) Developed Nomogram based on multifactorial logistic regression analysis.

### Model Validation

Through 1000 Bootstrap resampling iterations, the training group’s AUC was 0.921 (95% CI 0.872–0.970), and the validation group’s AUC was 0.900 (95% CI 0.828–0.972) (Figure 4). Demonstrating good predictive performance, the model is detailed in Table 3 and Supplementary Figure S1. Calibration curves for both groups exhibited well-fitted relationships between observed and predicted values (Figure 4). The Hosmer-Lemeshow goodness-of-fit test showed good fit in the training group with  $\chi^2 = 5.638$ ,  $P = 0.688$ , and in the validation group with  $\chi^2 = 6.259$ ,  $P = 0.618$ .

**Table 2** Multivariate Logistic Regression Analysis

Variables	B	S.E	P	OR	OR 95% CI	
					Lower	Upper
Diabetes	3.166	0.956	0.001	23.712	3.912	180.958
Modic change						
Normal	REF					
Type II	1.975	0.720	0.006	7.207	1.828	32.625
Type III	3.059	1.480	0.039	21.297	0.749	406.290
Ipsilesional multifidus SMI	-0.015	0.004	<0.001	0.985	0.977	0.992

**Abbreviations:** SMI, Skeletal Muscle Index; REF, Reference standard.

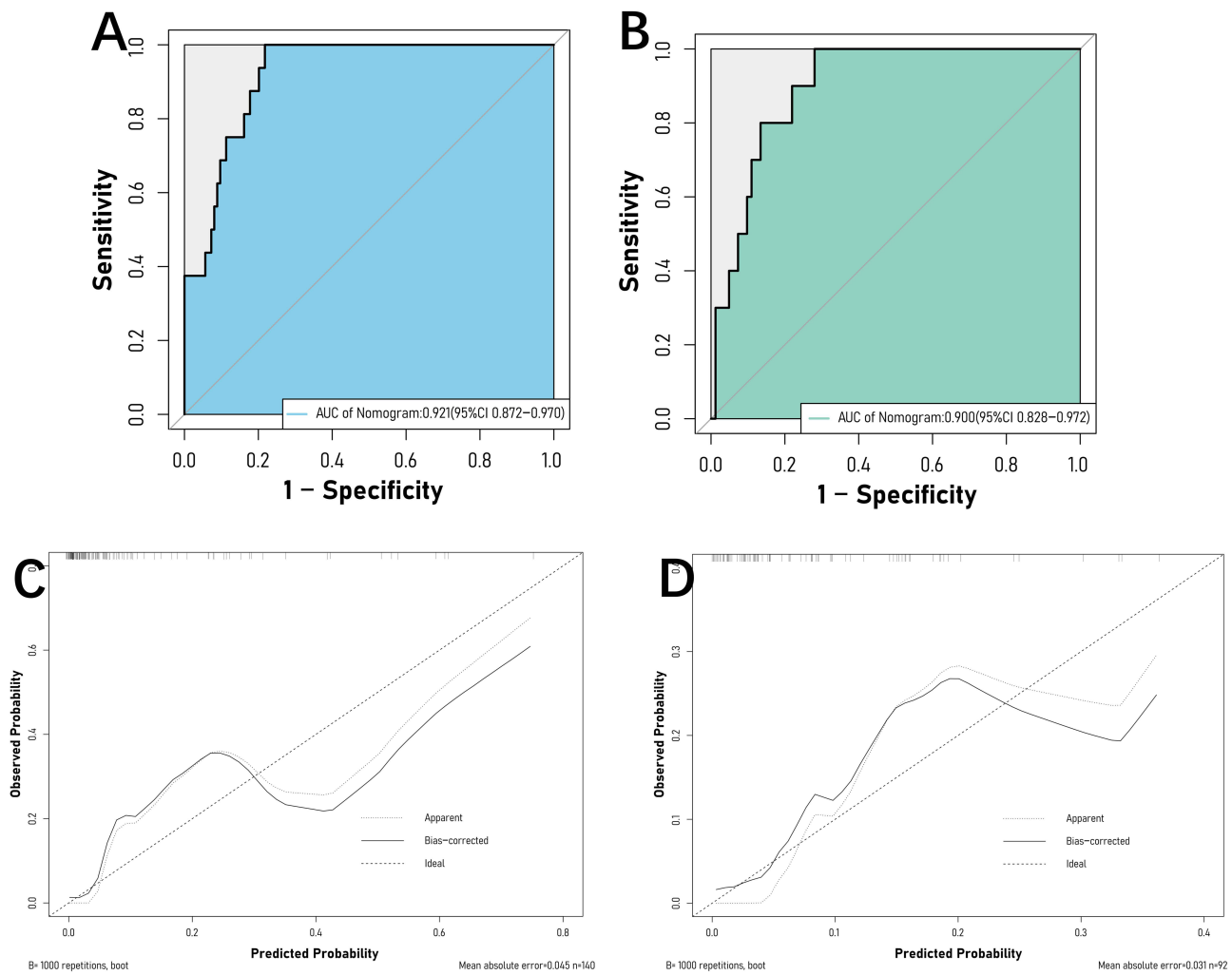


**Figure 4 (A and B)** The ROC curves of the training and validation groups exhibit AUC values of 0.921 (95% CI 0.872–0.970) and 0.900 (95% CI 0.828–0.972), respectively. **(C and D)** Training and validation set calibration curves.

### Clinical Utility of the Predictive Model

According to DCA curve results in the training and validation groups, the predictive model yields the maximum clinical net benefit within risk thresholds of 0.02–1.00 and 0.02–0.80. It provides significant additional clinical net benefit in predicting PRLDH occurrence (Figure 5). Risk stratification for 1000 cases using CIC indicates (Figure 5) that within the threshold probability range, the predicted number of patients experiencing PRLDH consistently exceeds the actual occurrences.

**Table 3** Diagnostic Performance of the Nomogram and Ipsilesional Multifidus SMI Model for Predicting PRLDH

Parameter	Training Set		Validation Set	
	Nomogram	Ipsilesional Multifidus SMI	Nomogram	Ipsilesional Multifidus SMI
AUC	0.921 (0.872, 0.970)	0.785 (0.678, 0.893)	0.900 (0.828, 0.972)	0.835 (0.727, 0.943)
Accuracy	0.807 (0.732, 0.869)	0.750 (0.670, 0.819)	0.739 (0.637, 0.825)	0.750 (0.649, 0.835)
Sensitivity	1.000 (0.794, 1.000)	0.688 (0.413, 0.890)	0.900 (0.55, 1.00)	0.900 (0.555, 0.997)
Specificity	0.782 (0.699, 0.851)	0.758 (0.673, 0.830)	0.720 (0.609, 0.813)	0.732 (0.622, 0.824)
PPV	0.372 (0.230, 0.533)	0.268 (0.142, 0.429)	0.281 (0.137, 0.467)	0.290 (0.142, 0.480)
NPV	1.000 (0.963, 1.000)	0.949 (0.886, 0.983)	0.983 (0.911, 1.000)	0.984 (0.912, 1.000)

**Abbreviations:** SMI, Skeletal Muscle Index = Paraspinal Muscle FCSA (mm<sup>2</sup>) / Height<sup>2</sup> (m<sup>2</sup>); PRLDH, Postoperative recurrent lumbar disc herniation; AUC, Area under the receiver operating characteristic curve; PPV, Positive Predictive Value; NPV, Negative Predictive Value.

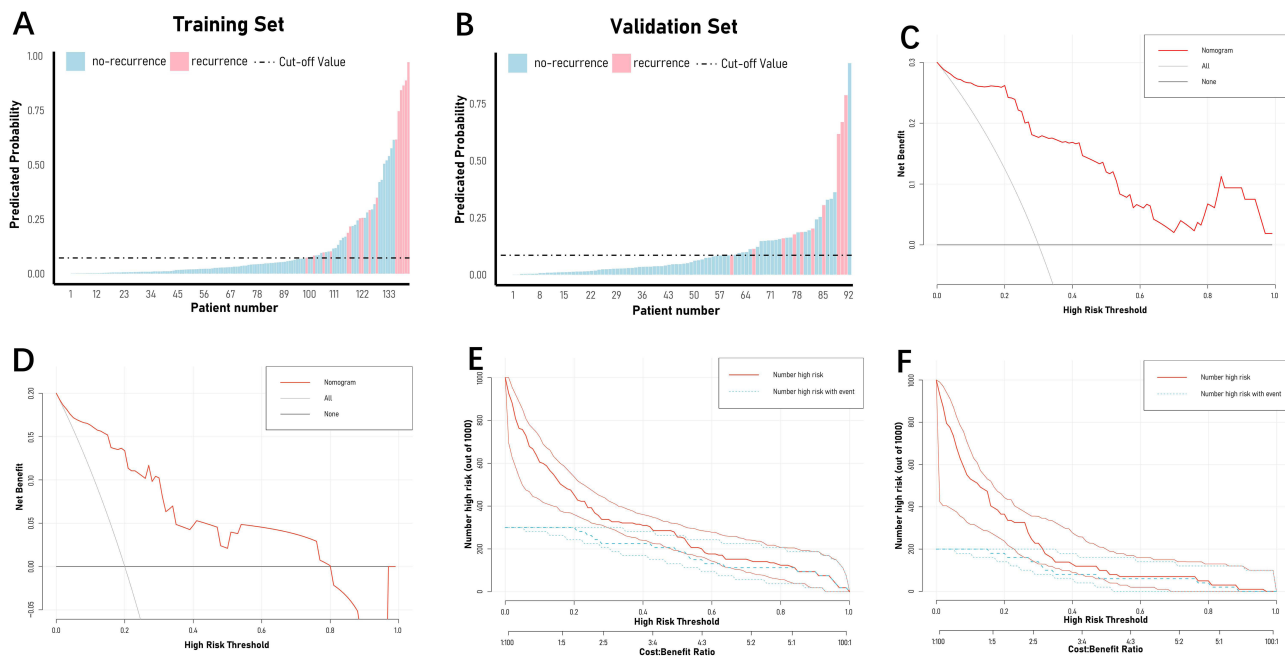


**Figure 5** (A and B) The prediction probability and the number of patients in the training set and the validation set of the nomogram, the dashed line indicates the cutoff value when the maximum Youden index is reached. (C and D) Decision Curve Analysis (DCA) curves for the training and validation sets. (E and F) Clinical Impact Curve (CIC) for the training and validation sets.

## Discussion

In our study, we identified diabetes, Modic changes, and ipsilesional multifidus SMI as independent predictors for PRLDH. The model demonstrated good predictive performance in both the training and validation sets. Meanwhile, the model's performance was unaffected by age ( $\geq 60$  years) (AUC: 0.914 vs 0.950;  $P = 0.491$ ) or gender (AUC: 0.915 vs 0.972;  $P = 0.146$ ) (Supplementary Table S4). The observed incidence of PRLDH in our study was 11.21%, aligning with the reported range in the literature (3–16%). In the current study, only a few have utilized paraspinal muscle parameters to predict PRLDH, primarily focusing on fat infiltration grades.<sup>21</sup> Quantitative studies on paraspinal muscles are as follows: Choi et al<sup>22</sup> conducted a retrospective analysis of 49 patients who underwent discectomy and partial laminectomy, revealing larger psoas major muscle parameters in PRLDH patients compared to those No-PRLDH. However, a larger study by Kong et al<sup>6</sup> (654 patients undergoing PETD) found smaller SFCSA at the L4/5 level in PRLDH patients (excluding the psoas major muscle), consistent with our findings. Nevertheless, previous studies have not explored the impact of different paraspinal muscles or asymmetry in paraspinal muscles on PRLDH occurrence. Our study demonstrates that paraspinal muscle SMI parameters can predict PRLDH occurrence, and we found no significant differences in contralesional and ipsilesional paraspinal muscle parameters among recurrent patients. However, most paraspinal muscle parameters in recurrent patients were significantly lower than those in non-recurrent patients, indicating pronounced paraspinal muscle degeneration (fat infiltration, fibrosis, and atrophy) in recurrent cases. Ipsilesional multifidus SMI may act as a protective factor against PRLDH. Its mechanism may involve nerve root injury resulting from disc herniation, leading to structural changes in ipsilateral paraspinal muscles, such as increased fat infiltration and type I to II fibers conversion. These changes may contribute to lower back pain and declining spinal function.<sup>23</sup> Therefore, prompt relief of nerve root compression is crucial for preserving paraspinal muscle mass, which not only alleviates patient discomfort but also improves prognosis.

Panjabi's<sup>8</sup> groundbreaking elucidation of the “three-system” theory and the concept of the “neutral zone” in spinal biomechanics has significantly advanced our understanding of the complexity and functional integration of the spinal structure. This has propelled research into other components of the spine, such as vertebral bodies, ligaments, and facet joints, enabling a better comprehension of the intricacies of lumbar spine disorders. Among these structures, paraspinal



muscles play a crucial role in maintaining spinal stability, particularly in the “neutral zone” and lumbar stability. As a local stabilizer, the multifidus muscle accounts for at least 2/3 of maintaining the stability of the “neutral zone”, and when the muscle degenerates, it will reduce the ability to control the neutral zone, and pain improvement does not necessarily mean multifidus muscle function recovery, but multifidus muscle atrophy may be related to recurrent LBP.<sup>24,25</sup> According to Zhu et al’s<sup>26</sup> study, PRLDH is more likely to occur when the multifidus muscle at the herniation site exhibits moderate to severe fatty infiltration. Studies have shown that the physiological cross-sectional area (PCSA) of the lumbar multifidus muscle is larger than that of the erector spinae, enabling it to generate more force.<sup>27,28</sup> This is attributed to the muscle fiber composition (I, IIA, and IIX types) of the paraspinal muscles. Agten et al’s<sup>29</sup> study indicates that, compared to the erector spinae, the multifidus has significantly larger type I muscle fibers, highlighting its greater role in maintaining spinal stability. Meanwhile, multifidus muscles are crucial for stabilizing and controlling spinal movement.<sup>25</sup>

This study quantified paraspinal muscle FCSA and further calculated paraspinal muscle SFCSA and SMI to account for inter-individual differences. While muscle volume typically correlates with patient height, degeneration of the vertebral body can lead to a decrease in the CSA/vertebral body CSA ratio due to diffuse proliferation, potentially compromising the reliability of SFCSA measurements.<sup>30</sup>

In our study, Modic changes and diabetes were also considered as predictive factors. The vertebral endplate consists of a bony endplate and a cartilaginous endplate, where the bony endplate is formed by ossification of the vertebral surface epiphyseal plate, while the cartilaginous endplate consists of a central thin layer of translucent cartilage of the vertebral endplate. Modic changes are defined based on abnormal MRI alterations of the vertebral endplate and subchondral bone. Previous research has indicated that lumbar Modic changes may contribute to lower back pain.<sup>31</sup> Modic changes may imply a state of intense inflammation. According to Luo et al’s<sup>32</sup> research, the use of exosomes derived from normal cartilage endplate stem cells (N-Exos) and degenerated cartilage endplate stem cells (D-Exos) in rats demonstrated their impact on apoptosis in nucleus pulposus cells and IVDD. They found that N-Exos were more effective in activating autophagy to suppress IVDD compared to D-Exos. Additionally, normal cartilage endplate stem cells inhibited apoptosis in nucleus pulposus cells by suppressing the inflammatory response. Both cartilage endplate degeneration and nucleus pulposus cell apoptosis are significant triggers of IVDD. When herniated material is exposed to body fluids, it triggers an inflammatory response, leading to the deterioration of the intervertebral disc microenvironment. Moreover, surgical procedures can damage the vertebral endplate, further exacerbating the microenvironment deterioration, thereby increasing the risk of PRLDH occurrence.

A meta-analysis by Luo et al<sup>33</sup> involving 58 cohort studies revealed a significant association between PRLDH and diabetes. This correlation may be linked to diabetes’ impact on the body’s connective tissues. Kakadiya et al<sup>34</sup> conducted a study on intervertebral disc tissues of diabetic patients using histopathological and immunofluorescence analysis, and observed reduced proteoglycan synthesis, increased aggrecan cleavage, and elevated expression of ADAMTS4/5 proteins (involved in proteoglycan breakdown within the intervertebral disc). These findings indicate that hyperglycemia accelerates apoptosis in intervertebral disc tissues. Meanwhile, an animal study demonstrated that high glucose increases stress-induced senescence (p16-pRB) pathway-related protein expression in a dose- and time-dependent manner, leading to senescence of nucleus pulposus cells in adult rats.<sup>35</sup> In conclusion, our developed Nomogram predictive model indicates that a smaller SMI of ipsilesional erector spinae or multifidus muscles, higher Modic change grade, and the presence of diabetes significantly increase the risk of PRLDH occurrence.

This study has several limitations. Firstly, this study is a single-center retrospective study. Although we performed internal validation using the training group, validation group, and enhanced Bootstrap method, additional clinical cohorts are needed for external validation. Secondly, we only included three predictive variables, while many other factors such as physical activity and inflammatory responses were not considered. Future research should address these limitations and further explore the impact of additional relevant factors.

## Conclusion

This study found differences in paraspinal muscle parameters between recurrent and non-recurrent patients, with no significant asymmetry observed in the contralesional and ipsilesional parameters of recurrent patients. Moreover, ipsilesional multifidus SMI was identified as a protective factor for PRLDH occurrence. Finally, the Nomogram predictive model, developed based on paraspinal muscle parameters in this study, demonstrates excellent predictive capability, facilitating risk assessment for the occurrence of PRLDH after PETD.

## Ethics Approval and Consent to Participate

This study adhered to the Declaration of Helsinki. Ethical approval (2023-keyan-062) was obtained from the Medical Ethics Committee of Hefei Hospital Affiliated to Anhui Medical University, with a waiver for written informed consent. Each patient signed an informed consent at the initiation of diagnosis, allowing for further clinical researcher using the clinical records. Moreover, the staff involved in this study have signed confidentiality agreements, ensuring full protection of all patients' privacy and personal identity information, with a strict commitment to non-disclosure.

## Acknowledgments

We sincerely thank Mr. Zhu and Mr. Shen for his invaluable assistance in image diagnosis.

## Funding

This work was supported by the Postgraduate Innovation Research and Practice Program of Anhui Medical University (No. YJS20230207). The institution played no role in the study design, data collection, analysis and interpretation, or manuscript writing.

## Disclosure

The authors declared no potential conflicts of interest with respect to the research, authorship, and/or publication of this article.

## References

- Zhang YG, Guo TM, Guo X, Wu SX. Clinical diagnosis for discogenic low back pain. *Int J Biol Sci*. 2009;5:647–658. doi:10.7150/ijbs.5.647
- Rajasekaran S, Bajaj N, Tubaki V, Kanna RM, Shetty AP ISSLS prize winner: the anatomy of failure in lumbar disc herniation: an in vivo, multimodal, prospective study of 181 subjects. *Spine*. 2013;38(17):1491–1500. doi:10.1097/BRS.0b013e31829a6fa6
- Djuric N, Yang X, Ostelo RWJG, et al. Disc inflammation and modic changes show an interaction effect on recovery after surgery for lumbar disc herniation. *Eur Spine J*. 2019;28:2579–2587. doi:10.1007/s00586-019-06108-9
- Basic Research and Transformation Society, Professional Committee of Spine and Spinal Cord, Chinese Association of Rehabilitation Medicine. Guideline for diagnosis, treatment and rehabilitation of lumbar disc herniation. *Zhonghua Wai Ke Za Zhi*. 2022;60(5):401–408. doi:10.3760/cma.j.cn112139-20211122-00548
- Yin S, Du H, Yang W, Duan C, Feng C, Tao H Prevalence of recurrent herniation following percutaneous endoscopic lumbar discectomy: a meta-analysis. *Pain Physician*. 2018;21(4):337–350.
- Kong M, Xu D, Gao C, et al. Risk factors for recurrent L4-5 disc herniation after percutaneous endoscopic transforaminal discectomy: a retrospective analysis of 654 cases. *Risk Manag Healthc Policy*. 2020;13:3051–3065. doi:10.2147/RMHP.S287976
- Kim CH, Chung CK, Choi Y, et al. The long-term reoperation rate following surgery for lumbar herniated intervertebral disc disease: a nationwide sample Cohort study with a 10-year follow-up. *Spine*. 2019;44(19):1382–1389. doi:10.1097/BRS.0000000000003065
- Panjabi MM. The stabilizing system of the spine. Part I. Function, dysfunction, adaptation, and enhancement. *J Spinal Disord*. 1992;5(4):383–389, 397. doi:10.1097/00002517-199212000-00001
- Crisco JJ, Panjabi MM, Yamamoto I, Oxland TR Euler stability of the human ligamentous lumbar spine. Part II: experiment. *Clin Biomech*. 1992;7(1):27–32. doi:10.1016/0268-0033(92)90004-N
- Schweitzer L, Geisler C, Pourhassan M, et al. What is the best reference site for a single MRI slice to assess whole-body skeletal muscle and adipose tissue volumes in healthy adults? *Am J Clin Nutr*. 2015;102(1):58–65. doi:10.3945/ajcn.115.111203
- Wassenaar M, van Rijn RM, van Tulder MW, et al. Magnetic resonance imaging for diagnosing lumbar spinal pathology in adult patients with low back pain or sciatica: a diagnostic systematic review. *Eur Spine J*. 2012;21(2):220–227. doi:10.1007/s00586-011-2019-8
- Cheng Z, Li Y, Li M, et al. Correlation between posterior paraspinal muscle atrophy and lumbar intervertebral disc degeneration in patients with chronic low back pain. *Int Orthop*. 2023;47(3):793–801. doi:10.1007/s00264-022-05621-9
- Kalichman L, Carmeli E, Been E. The association between imaging parameters of the paraspinal muscles, spinal degeneration, and low back pain. *Biomed Res Int*. 2017;2017:2562957. doi:10.1155/2017/2562957
- Kim HS, You JD, Ju CI. Predictive scoring and risk factors of early recurrence after percutaneous endoscopic lumbar discectomy. *Biomed Res Int*. 2019;2019:6492675. doi:10.1155/2019/6492675

15. Stanuszek A, Jędrzejek A, Gancarczyk-Urlik E, et al. Preoperative paraspinal and psoas major muscle atrophy and paraspinal muscle fatty degeneration as factors influencing the results of surgical treatment of lumbar disc disease. *Arch Orthop Trauma Surg.* 2022;142(7):1375–1384. doi:10.1007/s00402-021-03754-x
16. Jorgensen MJ, Marras WS, Gupta P. Cross-sectional area of the lumbar back muscles as a function of torso flexion. *Clin Biomech.* 2003;18(4):280–286. doi:10.1016/S0268-0033(03)00027-5
17. Lee ET, Lee SA, Soh Y, Yoo MC, Lee JH, Chon J. Association of lumbar paraspinal muscle morphometry with degenerative spondylolisthesis. *Int J Environ Res Public Health.* 2021;18(8):4037. doi:10.3390/ijerph18084037
18. Tang M, Wang S, Wang Y, et al. Development and validation of a nomogram predicting postoperative recurrent lumbar disc herniation based on activity factors. *Risk Manag Healthc Policy.* 2024;17:689–699. doi:10.2147/RMHP.S453819
19. Peduzzi P, Concato J, Kemper E, Holford TR, Feinstein AR. A simulation study of the number of events per variable in logistic regression analysis. *J Clin Epidemiol.* 1996;49(12):1373–1379. doi:10.1016/S0895-4356(96)00236-3
20. Schober P, Boer C, Schwarte LA. Correlation coefficients: appropriate use and interpretation. *Anesth Analg.* 2018;126(5):1763–1768. doi:10.1213/ANE.0000000000002864
21. Karadag MK, Akinci AT, Basak AT, et al. Preoperative magnetic resonance imaging abnormalities predictive of lumbar herniation recurrence after surgical repair. *World Neurosurg.* 2022;165:e750–e756. doi:10.1016/j.wneu.2022.06.143
22. Choi TY, Chang MY, Lee SH, Cho JG, Lee S. Psoas muscle measurement as a predictor of recurrent lumbar disc herniation: a retrospective blind study. *Medicine.* 2022;101:e29778.
23. Carvalho V, Santos J, Santos Silva P, Vaz R, Pereira P. Relationship between fatty infiltration of paraspinal muscles and clinical outcome after lumbar discectomy. *Brain Spine.* 2022;2:101697. doi:10.1016/j.bas.2022.101697
24. Freeman MD, Woodham MA, Woodham AW. The role of the lumbar multifidus in chronic low back pain: a review. *PM R.* 2010;2(2):142–146, 1–167. doi:10.1016/j.pmrj.2009.11.006
25. Noonan AM, Brown S. Paraspinal muscle pathophysiology associated with low back pain and spine degenerative disorders. *JOR Spine.* 2021;4:e1171.
26. Zhu F, Jia D, Zhang Y, et al. Moderate to severe multifidus fatty atrophy is the risk factor for recurrence after microdiscectomy of lumbar disc herniation. *Neurospine.* 2023;20(2):637–650. doi:10.14245/ns.2346054.027
27. Delp SL, Suryanarayanan S, Murray WM, Uhlir J, Triolo RJ. Architecture of the rectus abdominis, quadratus lumborum, and erector spinae. *J Biomech.* 2001;34(3):371–375. doi:10.1016/S0021-9290(00)00202-5
28. Ward SR, Kim CW, Eng CM, et al. Architectural analysis and intraoperative measurements demonstrate the unique design of the multifidus muscle for lumbar spine stability. *J Bone Joint Surg Am.* 2009;91(1):176–185. doi:10.2106/JBJS.G.01311
29. Agten A, Stevens S, Verbrugghe J, Eijnde BO, Timmermans A, Vandenabeele F. The lumbar multifidus is characterised by larger type I muscle fibres compared to the erector spinae. *Anat Cell Biol.* 2020;53(2):143–150. doi:10.5115/acb.20.009
30. Chang MY, Park Y, Ha JW, et al. Paraspinal lean muscle mass measurement using spine MRI as a predictor of adjacent segment disease after lumbar fusion: a propensity score-matched case-control analysis. *AJR Am J Roentgenol.* 2019;212(6):1310–1317. doi:10.2214/AJR.18.20441
31. Saukkonen J, Määttä J, Oura P, et al. Association between modic changes and low back pain in middle age: a northern Finland birth cohort study. *Spine.* 2020;45(19):1360–1367. doi:10.1097/BRS.0000000000003529
32. Luo L, Jian X, Sun H, et al. Cartilage endplate stem cells inhibit intervertebral disc degeneration by releasing exosomes to nucleus pulposus cells to activate akt/autophagy. *Stem Cells.* 2021;39(4):467–481. doi:10.1002/stem.3322
33. Luo M, Wang Z, Zhou B, et al. Risk factors for lumbar disc herniation recurrence after percutaneous endoscopic lumbar discectomy: a meta-analysis of 58 cohort studies. *Neurosurg Rev.* 2023;46(1):159. doi:10.1007/s10143-023-02041-0
34. Kakadiya G, Gohil K, Gandbhir V, et al. Hyperglycemia and its influence on development of lumbar degenerative disc disease. *N Am Spine Soc J.* 2020;2:100015. doi:10.1016/j.nxsj.2020.100015
35. Kong JG, Park JB, Lee D, Park EY. Effect of high glucose on stress-induced senescence of nucleus pulposus cells of adult rats. *Asian Spine J.* 2015;9(2):155–161. doi:10.4184/asj.2015.9.2.155